construction materials

MDPI

Article

Experimental Evaluation and Model-Assisted Multi-Objective Optimization of Semi-Dry Alkali-Activated Paving Units Containing Tailings and EAF Steel Slag

Meysam Azarsa [1], Iman Faridmehr [2,3,*] and Iman Varjavand [1]

[1] Department of Civil Engineering, Dez.C., Islamic Azad University, Dezful 6461645169, Iran
[2] Department of Civil Engineering, College of Engineering, University of Buraimi, Al Buraimi 512, Oman
[3] EcoStruct Building Technologies B.V., Fluwelen Burgwal 58, 2511 CJ The Hague, The Netherlands
* Correspondence: iman.f@uob.edu.om

Abstract

Iron-ore tailings (IOT) were evaluated as a fine solid constituent in semi-dry alkali-activated paving mixtures containing electric arc furnace (EAF) steel slag. Seventeen unique mixture formulations were evaluated through 19 experimental batches, including three independent center-condition batches, with 50–80% IOT in a fixed 500 kg/m^3 IOT/EAF-steel-slag precursor, nominal NaOH molarity of 8–14 mol/L, and dry sodium-metasilicate-to-NaOH (SMS/NaOH) ratios of 1.50–3.00. For each batch, the reported compressive and flexural strengths were the arithmetic means of three specimens tested for each response. The units were formed by vibration and pressure, sealed at 23 ± 2 °C, and tested after three days. Measured compressive and flexural strengths ranged from 15.17 to 25.66 MPa and 2.41 to 3.14 MPa, respectively. A quadratic response surface fitted to the 19 batch-level compressive-strength responses gave R^2 = 0.9997 and RMSE = 0.054 MPa; because no independent validation data were available, the stationary-point prediction of 26.36 MPa is treated as model-based rather than experimentally confirmed. Discrete Pareto screening using measured strength and provisional cost/GWP indicators identified M11, M13, M15, and M17 as non-dominated experimental cases. M11 is reported as a representative compromise solution within the tested cases. The results apply to the tested materials and three-day conditions and do not establish paving-product conformity.

Keywords: iron-ore tailings; electric arc furnace steel slag; alkali-activated material; semi-dry paving unit; sodium metasilicate; compressive strength; flexural strength; response surface methodology; Pareto screening; embodied carbon

Check for updates

Received: 21 August 2026
Revised: 19 September 2026
Accepted: 20 September 2026
Published: 1 October 2026

Copyright: © 2026 by the authors. Licensee MDPI, Basel, Switzerland. This article is an open access article distributed under the terms and conditions of the Creative Commons Attribution (CC BY) license.

1. Introduction

1.1. Problem Context

Alkali-activated materials are formed when an aluminosilicate or calcium-aluminosilicate solid reacts with an alkaline source and produces hardened binding phases. Low-calcium systems are usually related to cross-linked N-A-S-H-type networks, while calcium-rich slag systems can produce C-(A)-S-H-type gels that help early strength. For this reason, the broad term alkali-activated material is more suitable than geopolymer for the mixed IOT/steel-slag system used in this study [1].

A conventional two-part system uses an alkaline solution prepared separately, whereas a strict one-part system dry-mixes the precursor and solid activator before adding water [2].

In this work, NaOH flakes and sodium metasilicate pentahydrate were weighed as solid alkaline materials, combined in dry conditions, and added to the dry-blended mineral solids before water addition, as described in Section 4.2. The procedure is therefore described consistently as solid-activated, semi-dry processing rather than solution activation.

Avoiding Portland cement and adding waste materials does not automatically prove an environmental benefit. Commercial sodium silicate can drive several environmental impacts, and thermal curing can add energy use that reduces some of the benefit from precursor replacement [3]. Cost and carbon results also change with electricity, transport, activator dosage, and the allocation method used for industrial by-products such as slag [4]. For this reason, measured mechanical results should be kept separate from modeled cost and carbon indicators in a material-development study.

Iron-ore tailings are difficult to use as a precursor because their mineralogy, particle size, residual reagents, and trace-element content depend on the deposit and beneficiation process [5]. High SiO_2 content does not mean the silica is reactive when much of it remains as crystalline quartz. Mechanical activation, calcination, hydrothermal treatment, or blending with a more reactive calcium-bearing material may be needed for early strength development [6].

Earlier studies on fly ash/IOT mixtures found that moderate IOT contents can densify the matrix, whereas higher replacement levels can dilute the reactive precursor and reduce workability or strength [7]. IOT has also been used in alkali-activated bricks, with performance dependent on activator chemistry and curing conditions [8]. In the present work, the IOT/EAF-steel-slag system is evaluated as a combined formulation because IOT reactivity is limited and the response also depends on the alkaline constituents and particle packing. Semi-dry vibro-pressure production further introduces low mobile water, particle packing, immediate demolding, and controlled curing. Studies on concrete pavers with IOT [9], recycled mineral powders [10], and recycled asphalt aggregate [11] show that mixture-level strength should ultimately be considered together with product-scale absorption, abrasion, dimensional behavior, and environmental screening.

The acceptance procedure depends on the intended market. ASTM C936/C936M covers solid concrete interlocking paving units and refers the sampling and testing work to related unit methods [12]. EN 1338 covers unreinforced cement-bound concrete paving blocks and includes requirements for mechanical behavior, abrasion, weathering, and dimensions [13]. These standards were prepared for cement-bound products. Their test procedures can be used to examine an alkali-activated unit, but conformity can only be claimed when the required unit geometry, conditioning, sample size, test method, and acceptance statistics are used.

1.2. Knowledge Gap and Objectives

IOT has been studied as an aggregate, filler, activated precursor, and material for brick production, while solid-activated slag binders and alkali-activated paving blocks have often been studied separately. In the present semi-dry system, the IOT fraction, nominal NaOH molarity, and dry SMS/NaOH ratio vary within the same design space, yet the cited literature does not evaluate this combination with provisional cost and cradle-to-gate GWP screening. This defines the specific research gap addressed here.

This study had three objectives. The first objective was to check whether useful three-day compressive and flexural strengths could be retained when the IOT fraction increased from 50% to 80% of the precursor. The second objective was to check whether nominal NaOH molarity and the dry SMS/NaOH ratio produced bounded response maxima instead of a continuous benefit. The third objective was to identify non-dominated experimental formulations that increased three-day compressive strength while decreasing

provisional cost and GWP. IOT use was kept as a design variable when selecting the trade-off solution. This screening identified mixtures for confirmation and was not used to certify a paving product.

2. Literature Review

2.1. Reaction Framework and Terminology

Geopolymer technology was developed from the reaction of suitable aluminosilicates in alkaline media, which forms three-dimensional inorganic networks [14]. Later terminology separated low-calcium geopolymer gels from the larger group of alkali-activated binders, which also includes calcium-rich slag systems [15]. Spectroscopic and microscopic studies show that several gel types can coexist and change with precursor chemistry, pore-solution composition, and curing history [16]. Therefore, one idealized geopolymerization equation cannot describe the present IOT/EAF-steel-slag blend. In this study, the observed strength is discussed as a combined result of dissolution, precipitation, particle packing, and space filling.

The role of IOT depends on how much silica and alumina can participate in the system. Properly graded IOT has been used to replace fine aggregate in ultra-high-performance concrete, and this replacement changed particle packing, water demand, and interfacial behavior [17]. Studies on conventional concrete also show that too much fine replacement can increase paste demand and reduce strength [18]. IOT masonry mortars show a similar result because particle grading and particle surface affect the mixture together with the nominal oxide composition [19]. These results support the use of the studied IOT as a characterized mineral addition, rather than assuming that all of its SiO_2 and Al_2O_3 contents act as reactive binder.

2.2. Iron-Ore Tailings in Alkali-Activated Binders

Direct alkali activation of untreated IOT is limited when its main phases remain crystalline. Studies using thermal cycles on fly ash/IOT blends reported benefits at moderate IOT contents, but part of this effect came from filler densification and thermal stability instead of complete reaction [7]. Mechanical or thermal treatment can increase surface area or disturb Si–O bonds, but these treatments also require energy. For this reason, some integrated recovery methods first separated residual iron and then used the silicate-rich fraction as a concrete addition [20].

At the product scale, the main question is whether the composite can form a continuous load-bearing matrix with acceptable transport behavior. Ultra-high-performance concrete containing IOT has shown controlled permeability when fine particles improve packing, while higher replacement reduces strength when the binder does not cover the added surface [21]. Concrete made with dam tailings also shows that a local waste material must be tested as a specific material and should not be treated as a general IOT source [22].

2.3. Solid Activators, Slag, and Sodium Metasilicate

Studies on solid-activated binders show that ambient-cured strength depends on the dissolution rate of the activator and the reactive part of the precursor. Sodium-silicate grade, modulus, and available water affect setting and early strength [23]. In slag mortar, synthetic sodium metasilicate produced higher strength than alternative silica sources that dissolved more slowly, although the alternative sources could reduce the environmental burden [24].

A one-part slag cement with pretreated paper sludge formed calcium aluminosilicate hydrate and hydrotalcite-like phases, while the unreacted solids also worked as filler [25]. Particle-packing optimization has produced dense, high-strength one-part slag mixtures [26], and tests under cold conditions show that slag-based one-part binders can

continue gaining strength even when low temperatures slow the dissolution process [27]. These studies used blast-furnace slag or similar reactive systems, so their reaction behavior cannot be directly applied to EAF steel slag because its crystalline phases and iron-oxide content are different. The comparison is only used to explain the expected roles of alkalinity, soluble silicate, water, and particle packing.

2.4. Alkali-Activated Paving Units

Research on alkali-activated paving units has changed from cast mortar samples to vibro-compacted products. Pavers made with fly ash and rice-husk ash developed useful strength, while higher contents of porous ash increased absorption and reduced abrasion resistance [28]. Vibro-compacted pervious pavers also showed that controlled carbonation can change strength and abrasion, although enough open porosity is still needed for water infiltration [29]. Another environmental study used recycled aggregate, mine tailings, and carbonation, but required equivalent functions and all process emissions to remain within the comparison boundary [30].

The studies listed in Table 1 show how the research moved from using IOT as an aggregate or brick material to paving products with controlled chemistry. Each study provides some of the required information, but the cited literature has not studied the exact semi-dry IOT/EAF-steel-slag/SMS/NaOH system and the factor range used in this work together.

Table 1. Selected studies defining the research context.

Year	Material System	Finding Relevant to This Study	Ref.
2014	IOT as fine aggregate in UHPC	Fine IOT can improve packing, but replacement must be balanced against workability and paste demand.	[17]
2015	Heat- and ambient-cured one-part binder	Solid sodium-silicate grade changes dissolution, setting, and strength.	[23]
2016	IOT geopolymer bricks	IOT can be incorporated in alkali-activated masonry when activator and curing are controlled.	[8]
2016	Fly ash geopolymer with IOT	Moderate IOT densified the matrix; higher IOT diluted the reactive precursor.	[7]
2016	IOT replacing fine aggregate	An optimum replacement was reported because fine content changed water demand and strength.	[18]
2017	Interlocking pavers with dam IOT	Technical and environmental evaluation included unit testing and leaching.	[9]
2018	One-part slag mortar with silica sources	Synthetic SMS dissolved rapidly and developed high strength, with an activator burden.	[24]
2018	Slag/paper-sludge one-part cement	C-(A)-S-H and hydrotalcite-like products formed; unreacted material also filled space.	[25]
2019	Recycled-powder paving blocks	Abrasion, dimensions, and absorption were examined in addition to strength.	[10]
2020	IOT in UHPC	Packing can lower permeability, but high replacement can reduce binder continuity.	[21]
2020	Pavers with recycled asphalt aggregate	Aggregate–paste compatibility and compaction affected strength and durability.	[11]
2021	Particle-packed one-part slag blends	Granular design and solid activation produced dense, high-strength matrices.	[26]
2021	IOT characterization review	Mineralogy and morphology vary by source and do not support generic IOT assumptions.	[5]

Table 1. *Cont.*

Year	Material System	Finding Relevant to This Study	Ref.
2022	Alkali-activated IOT bricks	The reported program reached 18.45 MPa and a minimum absorption of 12.6%.	[31]
2023	Life-cycle assessment of IOT binder	Allocation, energy, and avoided-burden assumptions changed the environmental result.	[32]
2024	Carbonated vibro-compacted AAM pavers	Controlled carbonation changed the strength–abrasion balance of pervious units.	[29]

2.5. Consolidated Knowledge Gap

The reviewed studies establish three points relevant to the present program. First, untreated crystalline IOT cannot be assumed to replace a reactive precursor on a one-to-one basis under ambient curing. Second, alkalinity, soluble silicate, calcium-bearing solids, and particle packing can support early matrix formation, but results from blast-furnace slag cannot be transferred directly to EAF steel slag. Third, paving-unit suitability requires more than compressive strength. These points leave a specific gap: the combined effect of IOT fraction, nominal NaOH molarity, and dry SMS/NaOH ratio has not been evaluated together for the semi-dry IOT/EAF-steel-slag system used here while keeping measured mechanical response distinct from provisional cost and GWP screening. The experimental program therefore focused on these bounded factors and explicitly states the product-level tests that remain required.

3. Materials and Methods

3.1. Iron-Ore Tailings

Iron-ore tailings were collected from the Andimeshk iron-concentrate operation of Paniya Parto Kahraba Co., Andimeshk, Iran. The producer describes the site as an iron-concentrate facility with a nominal yearly capacity of about 300,000 t [33]. Figure 1 shows the collection area and the production facility. The received material was visually fine and reddish-brown, and it was dried, deagglomerated, and stored in sealed containers before batching. No calcination, mechanochemical activation, or additional beneficiation was used.



(**a**)

Figure 1. *Cont.*



(**b**)

Figure 1. Provenance of the iron-ore tailings: (**a**) tailings collection area and (**b**) iron-concentrate production facility in Andimeshk, Iran.

3.1.1. Particle-Size Distribution

The supplied particle-size data classified the IOT as a mainly fine and non-plastic ML material under the Unified Soil Classification System [34]. Figure 2 shows that 55.7% of the particles were smaller than 0.075 mm, including 49.2% silt and 6.5% clay. Fine sand was 44.0%, medium sand was 0.3%, and no coarse sand was reported. The effective particle size was D10 = 0.004 mm. Therefore, the grading shows a silt-dominated tailing with a considerable fine-sand fraction and almost no medium- or coarse-sand content.

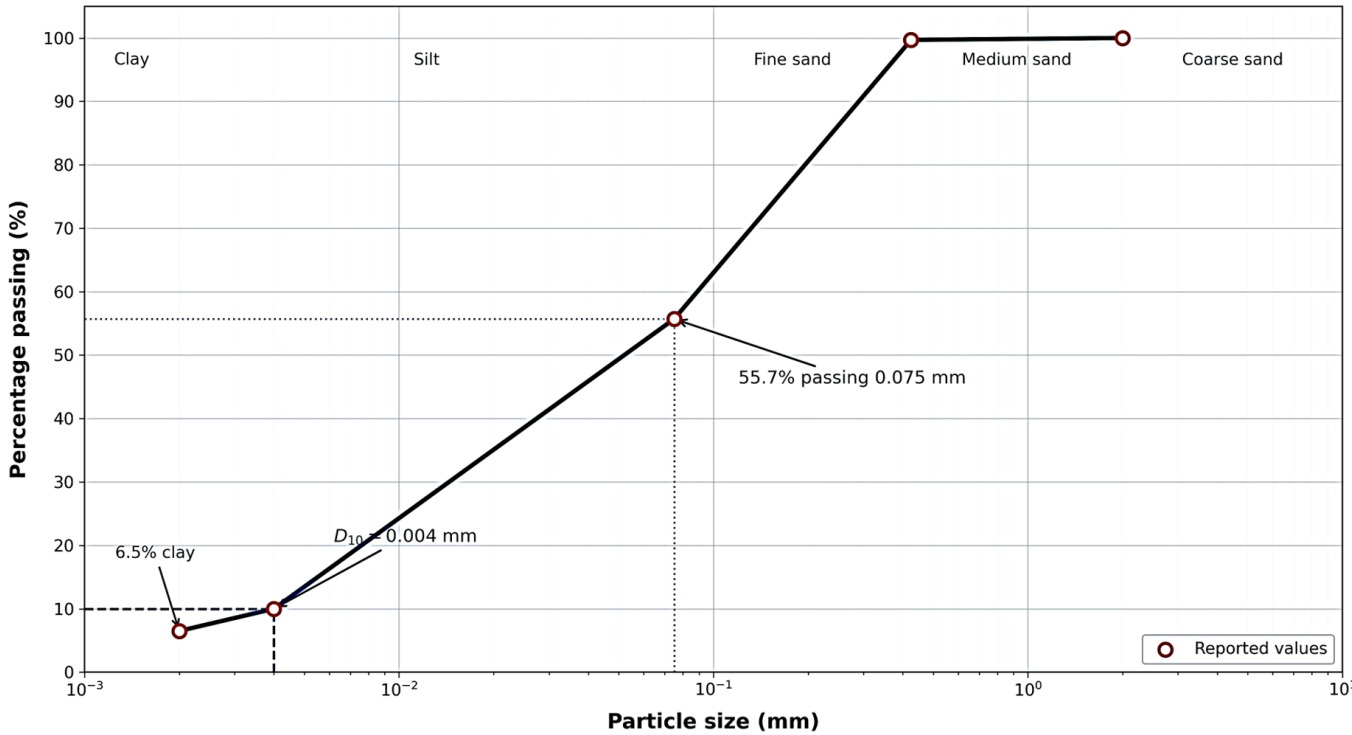


Figure 2. Particle-size distribution of the iron-ore tailings.

3.1.2. XRF Composition

Table 2 reproduces the supplied XRF reporting basis for five particle-size fractions. P, S, and Fe were reported as elemental values, whereas SiO_2, TiO_2, Al_2O_3, CaO, MgO, K_2O, MnO, and V_2O_5 were reported as oxides. Fe was the largest reported component and changed from 30.22% to 39.45%, with the highest value in the −38 + 5 µm fraction.

SiO_2 changed from 15.11% to 23.24%. The −5 µm fraction had the highest SiO_2 content and included 3.99% Al_2O_3 and 6.76% MgO, while its Fe content was 31.65%. CaO was between 5.43% and 7.88%, MgO was between 4.96% and 6.76%, and Al_2O_3 was between 2.63% and 4.09%. The differences between fractions show that the supplied composition was not uniformly distributed across particle sizes.

Table 2. XRF composition of the iron-ore tailings by particle-size fraction (%).

Component	−100 + 75 µm	−75 + 53 µm	−53 + 38 µm	−38 + 5 µm	−5 µm	Range
P	0.30	0.34	0.33	0.27	0.26	0.26–0.34
S	1.34	2.09	2.47	1.85	1.00	1.00–2.47
Fe	30.22	34.40	36.11	39.45	31.65	30.22–39.45
SiO_2	20.35	17.08	15.55	15.11	23.24	15.11–23.24
TiO_2	0.37	0.40	0.40	0.30	0.26	0.26–0.40
Al_2O_3	4.09	3.27	2.88	2.63	3.99	2.63–4.09
CaO	7.88	7.48	7.27	6.00	5.43	5.43–7.88
MgO	6.64	5.52	4.96	5.09	6.76	4.96–6.76
K_2O	0.32	0.22	0.17	0.14	0.22	0.14–0.32
MnO	0.06	0.07	0.07	0.06	0.07	0.06–0.07
V_2O_5	0.03	0.03	0.03	0.03	0.03	0.03

3.1.3. X-Ray Diffraction

Figure 3 is a supplied qualitative phase-reference map labeled for iron-ore tailings. It lists quartz, albite, talc, hematite, and calcite as reference phases.

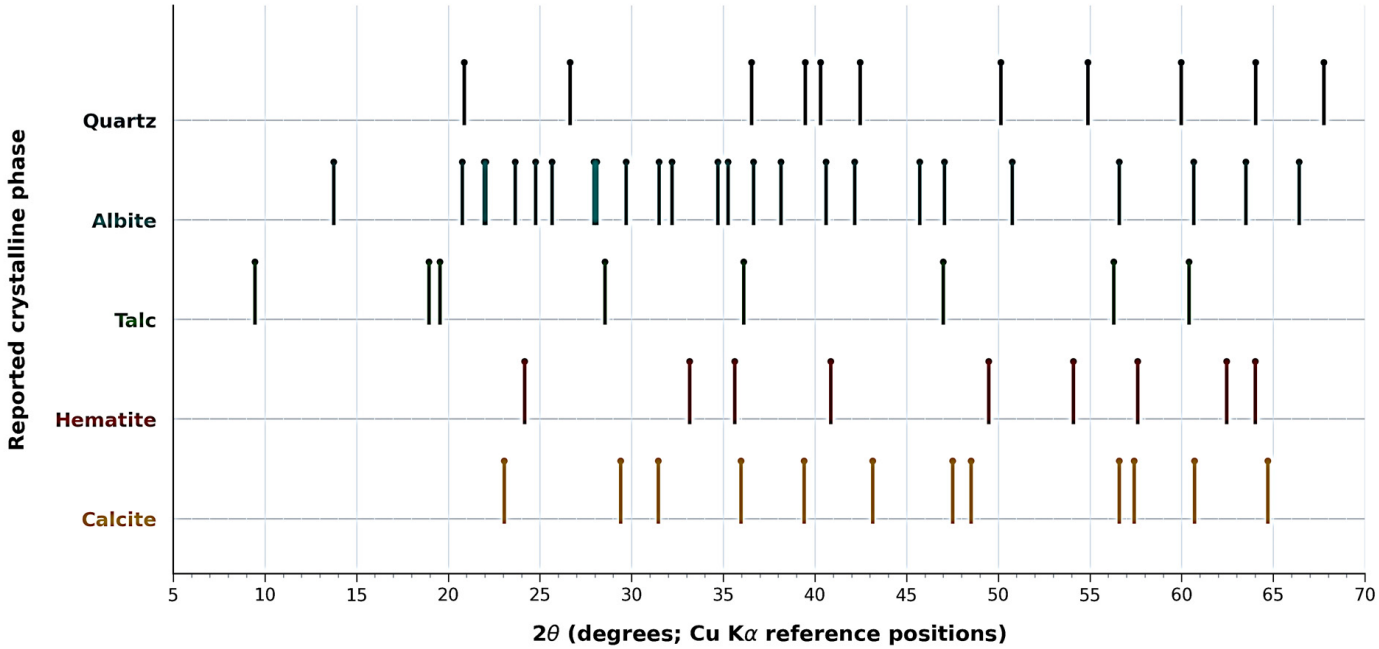


Figure 3. Qualitative phase-reference map labeled for iron-ore tailings.

Figure 4 is an XRD reference trace for iron-ore tailings; the sample had 43.09% total Fe and 12.1% FeO, while the calculated magnetite and hematite contents were 39% and 21.26%, respectively, and d80 was 66 µm [35].

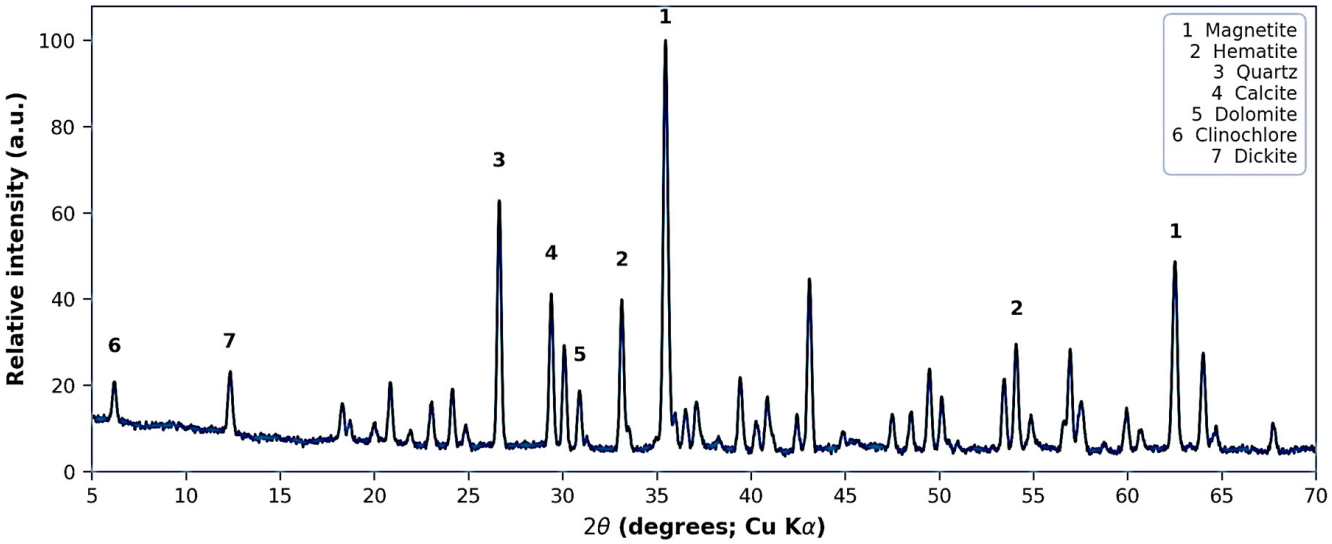


Figure 4. Redrawn and normalized XRD reference trace for iron-ore tailings, adapted from Ref. [35].

3.1.4. Leaching Record

The supplied leachate record for raw IOT reported the concentrations of nine elements. EPA SW-846 Method 1311 requires representative sampling, controlled extraction, filtration, chemical analysis, and related quality-control records [36]. Leaching behavior depends on the mineralogy, particle size, chemical composition, solution pH, and test conditions. These properties can also vary between IOT sources because the ore and beneficiation process differ [5]. The studied IOT mainly contained fine particles, but Figures 3 and 4 do not provide batch-specific mineralogical measurements. However, the present data do not show how these properties affected the release of the nine reported elements. The raw-IOT record also does not represent the behavior of the cured paving unit. Mixing the IOT with EAF steel slag and alkaline materials, followed by vibration, pressure, and curing, changes the material's physical and chemical conditions. Previous research on IOT pavers included leaching and dissolution tests on the produced units [9].

3.2. EAF Steel Slag

Electric arc furnace steel slag was collected from Mobarakeh Steel Company in Mobarakeh, Iran, and Figure 5 shows its supplied appearance. A published study on slag aggregate from the same steel complex reported rough and porous particles, bulk specific gravities of 3.05 and 2.95 for coarse and fine fractions, water absorptions of 1.8% and 2.1%, and a Los Angeles coefficient of 13.4% [37]. The published XRF composition included 38.86% CaO, 25.75% Fe_2O_3, 17.47% SiO_2, 5.01% MgO, and 4.03% Al_2O_3, and the calculated CaO/SiO_2 ratio was 2.22 [37].



Figure 5. EAF steel slag used in the mixture program.

Table 3 gives physical and chemical values for EAF steel slag from the same producer. The reported calcium-rich, iron-bearing composition also differs from conventional ground granulated blast-furnace slag, so reaction behavior from GGBFS systems is not transferred directly to the present material.

Table 3. Characteristics of EAF steel slag from Mobarakeh Steel Company. Data from [37].

Category	Characteristic	Published Value or Observation
Material	Production route	Electric arc furnace steel slag
Morphology	Particle surface	Rough, porous, and coarse-textured
Physical	Specific gravity	3.05 coarse; 2.95 fine
Physical	Water absorption	1.8% coarse; 2.1% fine
Physical	Los Angeles coefficient	13.4%
Chemical	Major XRF oxides	CaO 38.86%; Fe_2O_3 25.75%; SiO_2 17.47%
Chemical	Other reported oxides	MgO 5.01%; Al_2O_3 4.03%
Chemical	Calculated CaO/SiO_2 ratio	2.22

3.3. Alkaline Source

The alkaline source included sodium hydroxide flakes and solid sodium metasilicate pentahydrate ($Na_2SiO_3 \cdot 5H_2O$), as given in the supplier certificates [38,39], Table 4. The NaOH purity was 98.98%, and this value was used when a purity correction was needed. The reported Na_2CO_3, chloride, sulfate, and silicate contents were 1.00%, 150 ppm, 0.002%, and 0.001%, respectively. Sodium metasilicate was a white powder with 27.5 ± 1% Na_2O and 25.5 ± 1% SiO_2, and its 1% solution had a pH of 12.00 ± 0.5 at 25 °C. The pentahydrate formula was used in the bound-water calculation, and Figure 6 shows the physical appearance of the two solid alkaline materials.

Table 4. Supplier-reported properties of the alkaline constituents [38,39].

Property	Sodium Hydroxide Flakes	Sodium Metasilicate Pentahydrate
Chemical formula	NaOH	$Na_2SiO_3 \cdot 5H_2O$
Appearance	Flakes	White powder
Main chemical content	NaOH: 98.98%	Na_2O: 27.5 ± 1%; SiO_2: 25.5 ± 1%
pH of 1% solution at 25 °C	Not reported	12.00 ± 0.5
Reported impurities	Na_2CO_3: 1.00%; chloride: 150 ppm; sulfate: 0.002%; silicate as SiO_2: 0.001%	Not reported
Water-insoluble matter	None reported	Not reported



Figure 6. Solid alkaline constituents used in mixture preparation: (**a**) sodium metasilicate pentahydrate and (**b**) sodium hydroxide flakes.

3.4. Aggregates

Natural crushed aggregates were collected from an aggregate-processing plant in Andimeshk County, Khuzestan Province, Iran. Figure 7 shows the production plant and the separate aggregate fractions used for batching. The received particles were angular and were supplied in several size ranges.



Figure 7. Aggregate source and separated fractions: (**a**) production plant and (**b**) aggregate fractions used for mixture preparation.

3.5. Activator Accounting

Activator accounting was based on the actual dry-batched masses of sodium hydroxide flakes and sodium metasilicate pentahydrate. The dry SMS/NaOH mass ratio was defined as $R_A = \frac{m_{SMS}}{m_{NaOH}}$, and the total dry-batched activator mass was defined as $m_A = m_{NaOH} + m_{SMS}$. Equations (1) and (2) express the equivalent component relationships in terms of m_A and R_A. Accordingly, the total dry-batched activator was not fixed; it varied across batches.

$$m_{SMS} = m_A \frac{R_A}{1 + R_A} \quad (1)$$

$$m_{NaOH} = m_A \frac{1}{1 + R_A} \quad (2)$$

In Equations (1) and (2), m_{SMS} is the mass of sodium metasilicate pentahydrate, m_{NaOH} is the mass of sodium hydroxide flakes, m_A is the total dry-batched activator mass, and R_A is the dry SMS/NaOH mass ratio.

Nominal NaOH level was an experimental factor and was defined on the externally added-water basis. In Equation (3), the NaOH flake mass is obtained from the nominal NaOH level, the added-water volume basis, the NaOH molar mass, and the supplier-reported NaOH mass fraction. Equation (4) gives the stoichiometric water bound in $Na_2SiO_3 \cdot 5H_2O$.

$$m_{NaOH} = \frac{M_{NaOH} V_w M_{r,NaOH}}{p_{NaOH}} \quad (3)$$

$$m_{w,bound} = m_{SMS} \left(\frac{5 M_{r,H_2O}}{M_{r,Na_2SiO_3 \cdot 5H_2O}} \right) \quad (4)$$

In Equation (3), M_{NaOH} is the nominal NaOH level, V_w is the volume corresponding to the externally added water, $M_{r,NaOH}$ is the NaOH molar mass, and p_{NaOH} is the NaOH mass fraction. Bound water in $Na_2SiO_3 \cdot 5H_2O$ was accounted separately from the externally added water.

3.6. Curing Logic for Semi-Dry Units

The production method used vibro-pressure compaction followed by immediate demolding. Because the mobile-water content was low, early evaporation had to be controlled, so the units were sealed and cured at 23 ± 2 °C until the three-day test. A separate curing series at 40 ± 2 °C was not tested. Slag-containing alkali-activated mixtures can develop early strength during ambient curing [40], while precursor proportions and pore-solution chemistry affect the phase assemblage [41]. The activator type also affects reaction rate and gel development [42].

Figure 8 shows the proposed material and processing sequence. The diagram separates the supplied material properties, processing steps, and the proposed reaction stage.

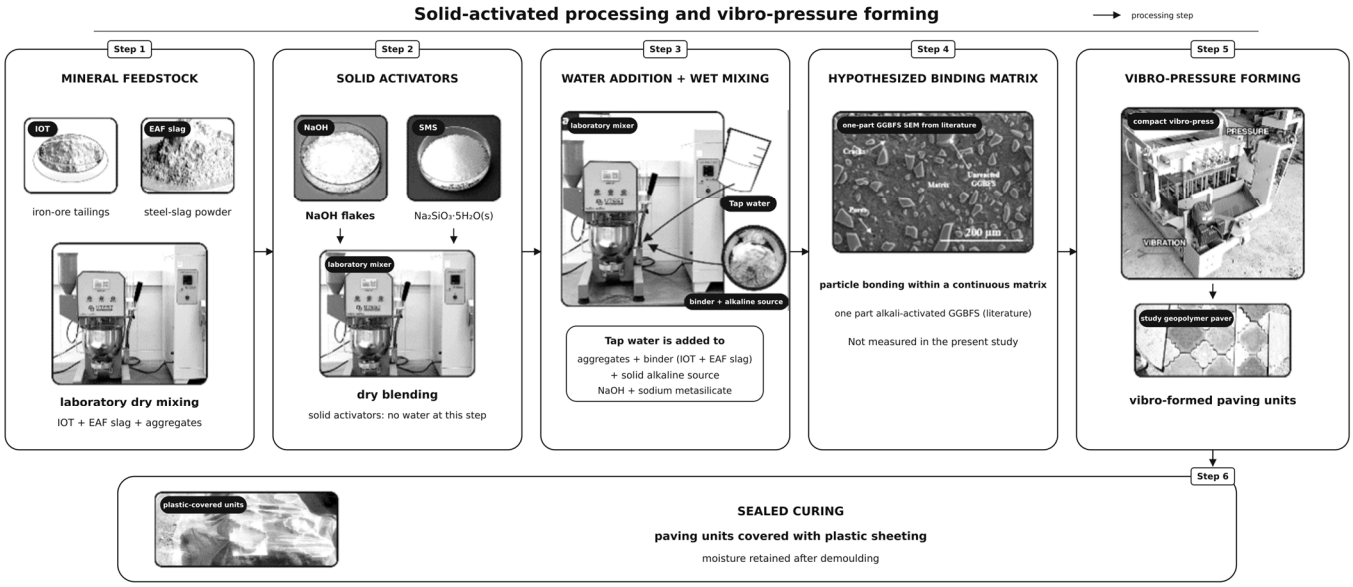


Figure 8. Proposed processing and reaction sequence for the IOT/EAF-steel-slag/SMS/NaOH semi-dry paving system.

3.7. Product Performance, Cost, and Environmental Accounting

ASTM C936/C936M has historically required an average compressive strength of at least 55 MPa for concrete interlocking paving units, while ASTM C140/C140M gives the related specimen preparation and testing procedure [12,43,44]. EN 1338 uses tensile splitting and breaking-load requirements instead of one general beam-flexural requirement [13]. Beam flexural strength from ASTM C78/C78M can be used for material comparison, but it cannot replace the finished-unit test required by the selected paver standard [45]. A separate lower compressive-strength limit is not given only because a paving unit uses an alkali-activated binder or contains IOT, since acceptance depends on the selected product standard and the intended use [12,13].

The provisional cost and GWP were calculated for 1 m^3 of mixture, which gave the same comparison basis for all formulations. The cost calculation included the material quantities, unit prices, and manufacturing energy. The cradle-to-gate GWP calculation included material production, manufacturing energy, and material transport. For formulation j, Equations (5) and (6) give these two calculations.

$$C_j^* = \sum_i m_{ij} p_i + \sum_k E_{kj} p_{E,k} \quad (5)$$

$$GWP_j^* = \sum_i m_{ij} EF_i + \sum_k E_{kj} EF_{E,k} + \sum_i m_{ij} d_i EF_{tr,i} \quad (6)$$

In Equations (5) and (6), m_{ij} is the mass of constituent i in formulation j, p_i is its unit price, E_{kj} is manufacturing energy of type k, $p_{E,k}$ is the energy price, EF_i and $EF_{E,k}$ are the constituent and energy emission factors, di is transport distance, and $EF_{tr,i}$ is the transport emission factor. This study calculated the reported cost and GWP values using the available project-level inventory. However, these values are provisional comparative screening indicators and should not be interpreted as reproducible cost estimates or a complete ISO 14040/14044 life-cycle assessment [46,47].

3.8. Mechanical Tests

Three-day compressive and flexural strengths were measured during the experimental program. Table 5 gives these two mechanical responses. The experimental design comprised 17 unique mixture formulations evaluated through 19 experimental batches. M17-M19 were independent center-condition batches prepared with the same nominal formulation. For each batch, three specimens were tested for compressive strength and three specimens were tested for flexural strength, and the arithmetic mean of the three measurements was used as the batch-level response. Compressive strength was used to examine the axial response of the formulations, while flexural strength was used to examine their bending response.

Table 5. Three-day mechanical responses used in the experimental program.

Property	Test Age	Current Status	Method	Use in the Study
Compressive strength	3 d	Measured	ASTM C140/C140M [44]	Batch-level compressive-strength comparison
Flexural strength	3 d	Measured	ASTM C78/C78M [45]	Batch-level flexural-response comparison

Figure 9 presents the laboratory photographs, which show the mixing work, controlled-temperature equipment, and mechanical loading arrangement.

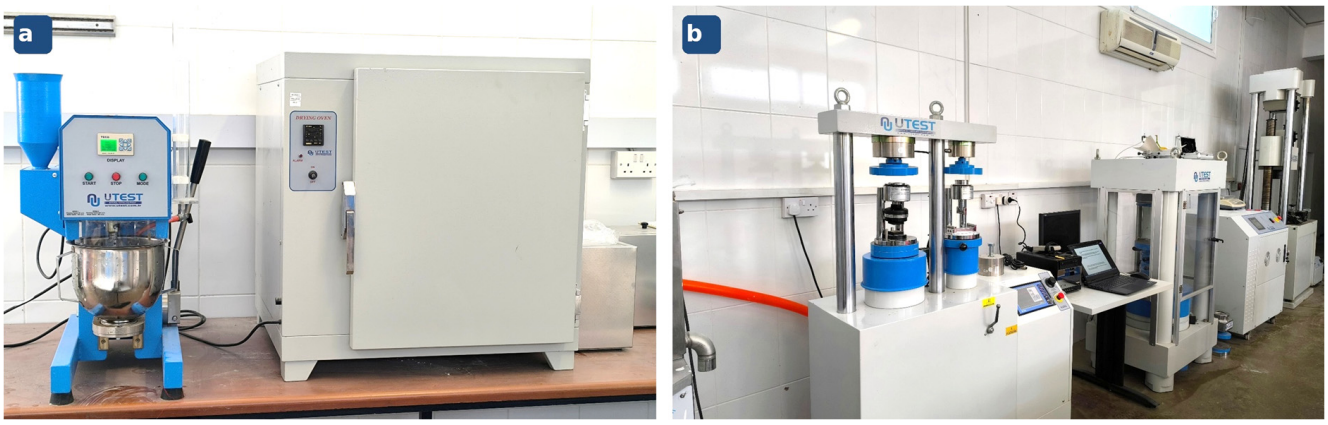


Figure 9. Laboratory processing and testing arrangements: (**a**) mixing/controlled-temperature equipment and (**b**) mechanical loading arrangement.

4. Experimental Program

4.1. Mixture Design and Factor Domain

Each experimental batch contained 500 kg/m^3 combined IOT and EAF steel slag, 1100 kg/m^3 fine aggregate, 550 kg/m^3 aggregate in the 2–8 mm fraction, and 30 kg/m^3 externally added water. The NaOH flake and SMS pentahydrate masses varied with the nominal NaOH level and dry SMS/NaOH ratio; consequently, the total dry-batched

activator varied from 24.25 to 67.89 kg/m^3. Equation (7) gives the fixed added-water-to-precursor ratio, while Equation (8) gives the observed range of the dry-batched-activator-to-precursor ratio. IOT replaced steel slag by mass inside the fixed 500 kg/m^3 precursor, so a change in IOT content did not change the total precursor mass. Aggregate grading should be reported using ASTM C136/C136M [48].

$$\frac{w_{\text{add}}}{P} = \frac{30}{500} = 0.060 \tag{7}$$

$$\frac{A_{dry}}{P} = \frac{24.25 - 67.89}{500} = 0.0485 - 0.1358 \tag{8}$$

In the experimental program, IOT content changed from 50% to 80% of the precursor, nominal NaOH molarity changed from 8 to 14 mol/L, and the dry SMS/NaOH ratio changed from 1.50 to 3.00. The center condition had 65% IOT, 11 mol/L NaOH, and RA = 2.25.

Table 6 gives all precursor and activator mass divisions used in the experimental design.

Table 6. Experimental batches and calculated precursor/activator splits (kg/m^3).

Mix	IOT (%)	IOT (kg/m^3)	EAF Slag (kg/m^3)	Nominal NaOH Level (mol/L of Added Water)	(R_A)	NaOH Flakes (kg/m^3)	SMS Pentahydrate (kg/m^3)	Total Dry-batched Activator (kg/m^3)	Added Water (kg/m^3)
M01	50	250	250	8	1.50	9.70	14.55	24.25	30.00
M02	50	250	250	10	2.50	12.12	30.31	42.43	30.00
M03	50	250	250	12	2.00	14.55	29.10	43.65	30.00
M04	50	250	250	14	3.00	16.97	50.92	67.89	30.00
M05	60	300	200	8	2.00	9.70	19.40	29.10	30.00
M06	60	300	200	10	3.00	12.12	36.37	48.49	30.00
M07	60	300	200	12	1.50	14.55	21.82	36.37	30.00
M08	60	300	200	14	2.50	16.97	42.43	59.41	30.00
M09	70	350	150	8	2.50	9.70	24.25	33.95	30.00
M10	70	350	150	10	1.50	12.12	18.19	30.31	30.00
M11	70	350	150	12	3.00	14.55	43.65	58.19	30.00
M12	70	350	150	14	2.00	16.97	33.95	50.92	30.00
M13	80	400	100	8	3.00	9.70	29.10	38.80	30.00
M14	80	400	100	10	2.00	12.12	24.25	36.37	30.00
M15	80	400	100	12	2.50	14.55	36.37	50.92	30.00
M16	80	400	100	14	1.50	16.97	25.46	42.43	30.00
M17	65	325	175	11	2.25	13.34	30.01	43.34	30.00
M18	65	325	175	11	2.25	13.34	30.01	43.34	30.00
M19	65	325	175	11	2.25	13.34	30.01	43.34	30.00

Every batch contained 30 kg/m^3 externally added water, 1100 kg/m^3 fine aggregate, and 550 kg/m^3 2–8 mm aggregate. SMS is commercial $Na_2SiO_3 \cdot 5H_2O$; therefore, its stoichiometric bound water was treated separately from the externally added water and can be calculated from Equation (4). Across Table 6, the bound-water contribution ranges from 6.18 to 21.62 kg/m^3. NaOH is reported as commercial flake mass. M17-M19 are independent center-condition batches prepared using the same nominal formulation. The 16 non-center formulations were arranged using a balanced 4 × 4 Latin-square-type design, in which each SMS/NaOH level occurred once at each IOT level and once at each NaOH level. Three additional independent batches were prepared at the center condition to assess repeatability and provide center-point information for the response-surface analysis.

4.2. Mixing, Forming, and Curing

The IOT and aggregates were dried to a controlled moisture condition before batching. The externally added water was maintained at 30 kg/m^3 for all batches. Water bound in $Na_2SiO_3 \cdot 5H_2O$ was not included in this added-water value.

IOT, EAF steel slag, aggregates, SMS, and NaOH were weighed.

NaOH was added to SMS in dry condition.

IOT, EAF steel slag, and aggregates were dry blended. The powder activator was added gradually, followed by the remaining water, until a visually coherent semi-dry mixture was obtained.

The mixture was placed in the paving-unit mold, compacted by vibration and pressure, struck level, and demolded.

The units were sealed within 10 min of demolding and cured at 23 ± 2 °C until the three-day test.

5. Results and Discussion

5.1. Manufactured Units and Performance Context

Figure 10 shows representative manufactured and installed paving units. The intact edges and laid surfaces show that immediate demolding and handling were possible for at least some of the batches.



Figure 10. Representative paving units and installed surfaces.

The available three-day strength values are below the 55 MPa minimum average for ASTM C936/C936M paving units [12,43]. The present measurements do not establish conformity with ASTM C936/C936M or EN 1338 because the test age and specimen information differ from the product procedures and several product-level acceptance tests were not conducted. The standard comparison is therefore used only as performance context.

5.2. Three-Day Compressive and Flexural Strength

Table 7 gives the measured responses and calculated screening indicators. Three-day compressive strength changed from 15.17 MPa for M13 and M16 to 25.66 MPa for M17, and the average of the 19 batch responses was 21.95 MPa. Flexural strength increased from 2.41 MPa for M13 and M16 to 3.14 MPa for M17, with an average of 2.90 MPa. Provisional cost ranged from 77.13 to 84.33 USD/m^3, while provisional GWP ranged from 82.59 to 93.84 kg CO_2-e/m^3. The cost and environmental values are model inputs based on an incomplete inventory, and they are not measured product properties.

Table 7. Measured three-day strengths and calculated screening indicators.

Mix	IOT (%)	M (mol/L)	RA	fc,3 (MPa)	fr (MPa)	Cost* (USD/m^3)	GWP* (kg CO_2-e/m^3)
M01	50	8	1.50	17.34	2.58	84.33	93.84
M02	50	10	2.50	23.99	3.04	83.99	92.12
M03	50	12	2.00	24.41	3.06	84.13	92.84
M04	50	14	3.00	24.00	3.04	83.88	91.59
M05	60	8	2.00	21.40	2.87	81.88	89.84
M06	60	10	3.00	23.97	3.04	81.63	88.59
M07	60	12	1.50	22.81	2.96	82.08	90.84
M08	60	14	2.50	25.15	3.11	81.74	89.12
M09	70	8	2.50	20.67	2.82	79.49	86.12
M10	70	10	1.50	21.06	2.85	79.83	87.84
M11	70	12	3.00	23.42	3.00	79.38	85.59
M12	70	14	2.00	22.21	2.92	79.63	86.84
M13	80	8	3.00	15.17	2.41	77.13	82.59
M14	80	10	2.00	19.45	2.73	77.38	83.84
M15	80	12	2.50	20.22	2.79	77.24	83.12
M16	80	14	1.50	15.17	2.41	77.58	84.84
M17	65	11	2.25	25.66	3.14	80.68	87.95
M18	65	11	2.25	25.34	3.12	80.68	87.95
M19	65	11	2.25	25.54	3.13	80.68	87.95

fc,3 and fr were measured at the batch-response level. Cost* and GWP* are provisional screening values; the unit-price and emission-factor inventory is incomplete.

Figure 11 shows that strength did not continuously decrease when the IOT content increased. At 50% IOT, strength increased from 17.34 MPa in M01 to about 24 MPa in M02–M04, while the values at 60% IOT were between 21.40 and 25.15 MPa. M11 gave 23.42 MPa at 70% IOT, 12 mol/L NaOH, and RA = 3.00, while M15 gave 20.22 MPa at 80% IOT, 12 mol/L, and RA = 2.50. Within the tested three-day range, these results answer the first objective because a higher IOT level could keep a moderate early strength, although the result also depended on the activator combination.

The flexural results followed the same general pattern as the compressive results in Figure 11. At 50% IOT, flexural strength was between 2.58 and 3.06 MPa, while the ranges were 2.87–3.11 MPa at 60% IOT, 2.82–3.00 MPa at 70% IOT, and 2.41–2.79 MPa at 80% IOT. M17 had the highest measured flexural strength of 3.14 MPa, while M13 and M16 both had 2.41 MPa. For the 19 batch-level paired responses in Table 7, flexural and compressive strengths had a strong association (Pearson r = 0.999). Each batch-level response was the arithmetic mean of three specimens for the corresponding mechanical test; therefore, the correlation was calculated from 19 paired batch means rather than individual specimen measurements. It describes the present dataset and does not provide a general conversion or prove a reaction mechanism.

At 80% IOT, M14 and M15 gave 19.45–20.22 MPa, while M13 and M16 both gave 15.17 MPa with opposite molarity–ratio combinations. Therefore, the same IOT content produced a strength range of 5.05 MPa. This difference suggests a possible interaction between hydroxide concentration and the silicate-to-hydroxide balance, but the experiment does not reveal the reaction mechanism. The lower EAF-slag fraction at 80% IOT may also reduce the amount of calcium-bearing reactive material, but the phase reaction and pore structure were not measured.



Figure 11. Measured three-day (**a**) compressive strength and (**b**) flexural strength for the 19 experimental batches representing 17 unique formulations; M17-M19 are independent center-condition batches, and dashed lines show the overall batch means.

The compressive strengths of the three center-condition batches were 25.66, 25.34, and 25.54 MPa. The average was 25.51 MPa, the sample standard deviation was 0.162 MPa, and the coefficient of variation was 0.63%. The related flexural strengths were 3.14, 3.12, and 3.13 MPa, while the average, sample standard deviation, and coefficient of variation were 3.13 MPa, 0.010 MPa, and 0.32%, respectively. Each reported batch-level strength represents the arithmetic mean of three specimens. The variation among M17-M19 therefore describes batch-to-batch repeatability at the center condition.

5.3. Comparison with Conventional and Alkali-Activated Paving Systems

Compared with conventional cement-bound paving systems, the principal potential advantage of the present formulation is the combined use of IOT and EAF steel slag as major solid constituents together with semi-dry vibro-pressure processing and ambient-temperature curing. This approach provides a route for incorporating industrial mineral residues without relying on Portland cement in the studied formulation. However, the measured three-day strengths remained below the cited paving-unit benchmark, and the cost and GWP values are provisional screening indicators. Therefore, the present data do not demonstrate superior mechanical, economic, or environmental performance over conventional or other alkali-activated paving technologies.

6. Multi-Objective Optimization

6.1. Response-Surface Formulation

The response-surface calculation was used in the optimization analysis. Table 8 was used to change the three experimental factors into the coded variables A, B, and C. A full second-order model was then fitted by least squares to the 19 batch-level three-day compressive-strength responses obtained from 17 unique formulations, including three independent center-condition batches, based on the response-surface form in [49].

Table 8. Factor bounds and coded-variable definitions used in the response-surface model.

Factor	Symbol	Low (−1)	Center (0)	High (+1)	Coding
IOT in precursor	A	50%	65%	80%	A = (IOT − 65)/15
Nominal NaOH molarity	B	8 mol/L	11 mol/L	14 mol/L	B = (M − 11)/3
Dry SMS/NaOH ratio	C	1.50	2.25	3.00	C = (RA − 2.25)/0.75

Equation (9) gives the general second-order relation. In this equation, A is IOT content, B is nominal NaOH molarity, and C is the dry SMS/NaOH ratio after coding.

$$f_{c,3} = \beta_0 + \beta_1 A + \beta_2 B + \beta_3 C + \beta_{12} AB + \beta_{13} AC + \beta_{23} BC + \beta_{11} A^2 + \beta_{22} B^2 + \beta_{33} C^2 \quad (9)$$

The measured batch responses were used to estimate the coefficients, and Equation (10) gives the fitted empirical relation.

$$f_{c,3} = 25.494 - 2.239A + 1.280B + 0.960C - 0.704AB - 0.385AC + 0.512BC \\ -2.955A^2 - 2.572B^2 - 2.057C^2 \quad (10)$$

The fitted relation represented the 19 batch-level calibration responses with $R^2 = 0.9997$ and RMSE = 0.054 MPa. These metrics describe calibration fit only. No independent data outside these 19 experimental batch responses were used for validation, and the stationary-point prediction was not experimentally confirmed. Accordingly, the equation is treated as an empirical response surface within the studied factor domain rather than an independently validated predictive model. Flexural strength was studied as a separate measured response, and ACI 318 [50] was not used to calculate it from compressive strength. The negative quadratic coefficients in Equation (10) show bounded curvature inside the coded factor range.

6.2. Multi-Objective Formulation and Pareto Screening

The discrete screening used the objectives of maximizing measured three-day compressive strength and minimizing provisional cost and provisional GWP. Equation (11) writes these objectives as a minimization vector. A formulation was non-dominated when no other tested formulation was equal or better for all three objectives and better for at least one objective. A weighted desirability function [51] was not used because the objective weights were not defined.

$$\mathbf{F}_j = \left[-f_{c,3,j}, |C_j^*, |GWP_j^* \right] \quad (11)$$

The workflow in Figure 12 was used with the measured strength and provisional indicators in Table 7. The non-dominated formulations were M11, M13, M15, and M17. M17 had the highest measured compressive strength of 25.66 MPa, with a provisional cost of 80.68 USD/m^3 and GWP of 87.95 kg CO_2-e/m^3. M13 had the lowest cost and GWP of 77.13 USD/m^3 and 82.59 kg CO_2-e/m^3, but its measured strength was 15.17 MPa. M15 gave 20.22 MPa at 77.24 USD/m^3 and 83.12 kg CO_2-e/m^3, while M11 gave 23.42 MPa at 79.38 USD/m^3 and 85.59 kg CO_2-e/m^3.

Figure 13 shows the tested formulations in the three-objective space. None of the non-dominated formulations had the best value for all objectives. M11 is identified as a representative compromise solution because it retained 70% IOT and had greater measured strength than M13 and M15, while its provisional cost and GWP were lower than those of M17. This selection is an engineering trade-off within the tested data and provisional inventory; it is not a universal optimum or an experimentally confirmed optimum.

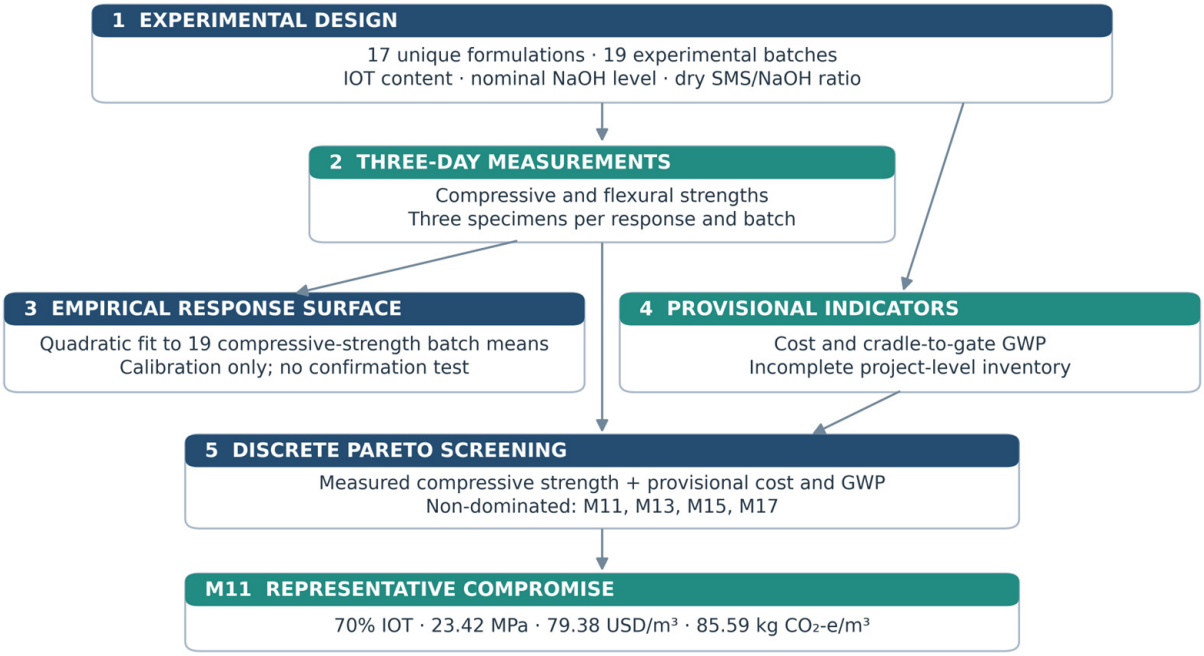


Figure 12. Calculation sequence used for response-surface fitting, Pareto screening, and selection of a representative compromise solution.

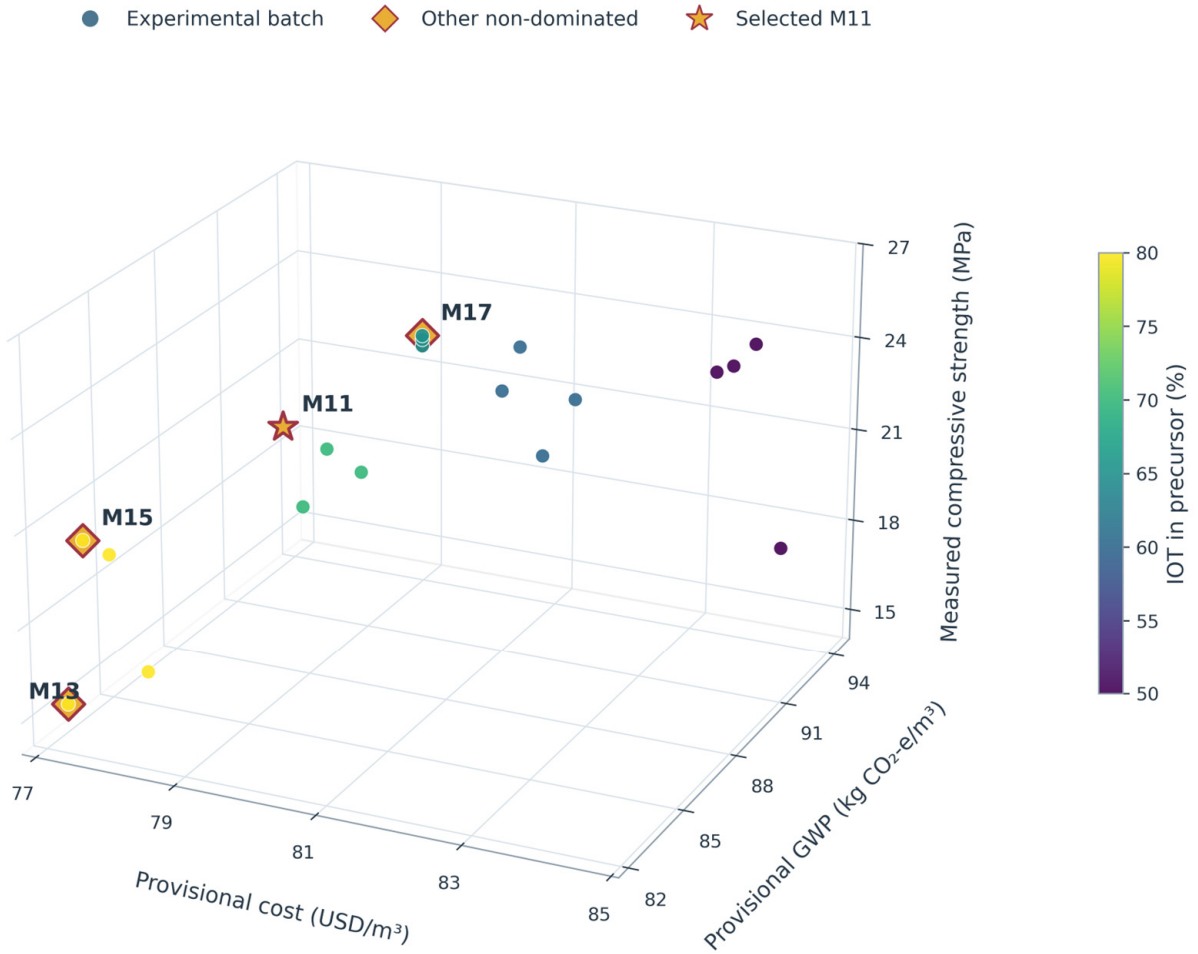


Figure 13. Three-dimensional distribution of measured three-day compressive strength, provisional cost, and provisional GWP. (Diamonds mark M13, M15, and M17; the star marks M11, which is also non-dominated and was selected as a representative compromise).

6.3. Empirical Calculation Procedure and Application Limits

For a candidate mixture, the original inputs are IOT content, nominal NaOH molarity, and the dry SMS/NaOH ratio. Equation (12) is first used to change these inputs to A, B, and C, and Equation (10) is then used for the calculation.

$$\begin{aligned} A &= \frac{X_{\mathrm{IOT}} - 65}{15}, \\ B &= \frac{M_{\mathrm{NaOH}} - 11}{3}, \\ C &= \frac{R_A - 2.25}{0.75} \end{aligned} \tag{12}$$

In Equation (12), X_{IOT} means IOT content in percent, M_{NaOH} means nominal NaOH molarity in mol/L, and R_{A} means the dry SMS/NaOH ratio. For M11, the input values of 70%, 12 mol/L, and 3.00 give A = 0.333, B = 0.333, and C = 1.000. Using these values in Equation (10), the fitted result is 23.43 MPa, while the measured result is 23.42 MPa. This comparison is only an internal calibration check and is not an independent validation.

The stationary point of the fitted surface was found by setting the first three derivatives of Equation (10) to zero, and Equation (13) shows the resulting linear system.

$$\begin{aligned} \frac{\partial f_{c,3}}{\partial A} &= -2.239 - 0.704B - 0.385C - 5.910A = 0, \\ \frac{\partial f_{c,3}}{\partial B} &= 1.280 - 0.704A + 0.512C - 5.144B = 0, \\ \frac{\partial f_{c,3}}{\partial C} &= 0.960 - 0.385A + 0.512B - 4.114C = 0 \end{aligned} \tag{13}$$

The solution of Equation (13) gave A = −0.440, B = 0.341, and C = 0.317. The inverse changes in Equation (12) gave 58.4% IOT, 12.02 mol/L nominal NaOH, and RA = 2.49. Using these values in Equation (10), the predicted three-day compressive strength was 26.36 MPa. This stationary point is inside the tested factor range but was not tested as an additional formulation; it is therefore a model prediction rather than an experimentally verified optimum.

For multi-objective use, Equations (5) and (6) are first used to calculate the cost and GWP of each candidate, and Equation (11) is then used to form the three-objective vector. Pairwise dominance is checked for all candidates. Because the complete price, energy, transport, allocation, and emission-factor inventory was unavailable, this Pareto screening is preliminary and uses only the provisional values reported in Table 7. It should not be interpreted as a reproducible life-cycle or cost assessment.

Equation (10) can only be used for 50–80% IOT in the precursor, 8–14 mol/L nominal NaOH, and a dry SMS/NaOH ratio of 1.50–3.00. It also represents only the studied materials, the mixture quantities reported in Table 6, the reported aggregates, vibro-pressure forming, sealed curing at 23 ± 2 °C, and a three-day test age. The available data do not support use of the equation outside these conditions or independent predictive validation.

7. Conclusions and Recommendations

7.1. Concluding Remarks

This study examined the three-day mechanical response and multi-objective trade-offs for 17 unique semi-dry IOT/EAF-steel-slag paving formulations evaluated through 19 experimental batches. The findings apply only to the tested materials, factor ranges, forming method, curing condition, and batch-level measurements; no paving-product conformity or independent model validation is claimed.

1. The measured three-day compressive strength was between 15.17 and 25.66 MPa, while the flexural strength was between 2.41 and 3.14 MPa. The three center-condition batches had average compressive and flexural strengths of 25.51 and 3.13 MPa, with coefficients of variation of 0.63% and 0.32%, respectively. Each batch-level mechanical response was the arithmetic mean of three specimens; the reported center-condition coefficients of variation therefore describe variation among the three independent batch means.

2. Strength did not continuously decrease as IOT content increased across the tested formulations. At 80% IOT, M15 gave 20.22 MPa compressive strength and 2.79 MPa flexural strength. Because IOT content, nominal NaOH molarity, and dry SMS/NaOH ratio changed together across the design, this result represents a combined formulation response and does not isolate the causal effect of IOT content alone.

3. For the 19 batch-level calibration responses, the quadratic compressive-strength model gave R^2 = 0.9997 and RMSE = 0.054 MPa. The stationary-point calculation predicted 26.36 MPa at 58.4% IOT, 12.02 mol/L nominal NaOH, and a dry SMS/NaOH ratio of 2.49. Because no independent validation or confirmation test was available, these values reflect calibration performance and model predictions within the tested factor domain.

4. The discrete Pareto set for measured compressive strength, provisional cost, and provisional GWP included M11, M13, M15, and M17. M11 is reported as a representative compromise solution because it combined 70% IOT and 23.42 MPa measured strength with provisional cost and GWP values of 79.38 USD/m^3 and 85.59 kg CO_2-e/m^3. The selection depends on the tested experimental cases and incomplete cost/GWP inventory and should not be interpreted as a universally optimal mixture.

7.2. Recommendations for Later Research

Later work should prepare independent batches of M11 and the predicted stationary formulation. Future reporting should include individual specimen values at three days and at later ages so that variation between batches and within each batch can be separated. Finished paving units should also be tested by using the geometry, conditioning, sampling, and acceptance procedures of the selected product standard.

The phase assemblage and reaction products should be studied by quantitative XRD, spectroscopy, and microscopy before C-(A)-S-H- or N-(C)-A-S-H-type products are assigned to the studied binder [52]. Product-level testing should also include water absorption and voids, abrasion, dimensional behavior, tensile splitting or breaking load, and freeze–thaw/de-icing-salt resistance using the applicable product and test standards [13,53,54].

A complete cost inventory and cradle-to-gate life-cycle inventory are needed before the provisional indicators are used for comparative claims. The inventory should include material prices, transport distances, electricity use, emission factors, activator production, and the allocation method for IOT and EAF slag, and it should follow the selected ISO 14040/14044 framework [46,47].

Author Contributions: Conceptualization, I.F. and M.A.; methodology, M.A., I.V. and I.F.; investigation and data curation, M.A. and I.V.; formal analysis, software and visualization, I.F.; writing—original draft preparation, I.F.; writing—review and editing, M.A., I.V. and I.F.; supervision, I.V. and I.F.; project administration, I.F. All authors have read and agreed to the published version of the manuscript.

Funding: This research received no external funding.

Data Availability Statement: The original contributions presented in this study are included in the article. Further inquiries can be directed to the corresponding author.

Acknowledgments: The authors thank the material manufacturers and laboratories that generated the batch certificates and characterization records.

Conflicts of Interest: Iman Faridmehr is the founder and Chief Executive Officer of EcoStruct Building Technologies B.V., a company developing low-carbon concrete solutions, He discloses this commercial role as a potential conflict of interest related to the manuscript. No grant or other external research funding was received for this work. He declares no other conflict of interest related to this work. Meysam Azarsa and Iman Varjavand declare that they have no financial or non-financial conflicts of interest related to this work.

Abbreviations

The following abbreviations are used in this manuscript:

AAM	Alkali-activated material
ACI	American Concrete Institute
ASTM	ASTM International
C-(A)-S-H	Calcium (alumino)silicate hydrate
CO_2-e	Carbon dioxide equivalent
EAF	Electric arc furnace
EN	European Standard
EPA	U.S. Environmental Protection Agency
GGBFS	Ground granulated blast-furnace slag
GWP	Global warming potential
IOT	Iron-ore tailings
ISO	International Organization for Standardization
ML	Inorganic silt of low plasticity (Unified Soil Classification System symbol)
N-A-S-H	Sodium aluminosilicate hydrate
N-(C)-A-S-H	Sodium (calcium) aluminosilicate hydrate
NaOH	Sodium hydroxide
SMS	Sodium metasilicate
UHPC	Ultra-high-performance concrete
USD	United States dollar
XRD	X-ray diffraction
XRF	X-ray fluorescence

References

1. Provis, J.L. Alkali-activated materials. *Cem. Concr. Res.* **2018**, *114*, 40–48. [CrossRef]
2. Luukkonen, T.; Abdollahnejad, Z.; Yliniemi, J.; Kinnunen, P.; Illikainen, M. One-part alkali-activated materials: A review. *Cem. Concr. Res.* **2018**, *103*, 21–34. [CrossRef]
3. Habert, G.; d'Espinose de Lacaillerie, J.B.; Roussel, N. An environmental evaluation of geopolymer based concrete production: Reviewing current research trends. *J. Clean. Prod.* **2011**, *19*, 1229–1238. [CrossRef]
4. McLellan, B.C.; Williams, R.P.; Lay, J.; van Riessen, A.; Corder, G.D. Costs and carbon emissions for geopolymer pastes in comparison to ordinary Portland cement. *J. Clean. Prod.* **2011**, *19*, 1080–1090. [CrossRef]
5. Zhao, J.; Ni, K.; Su, Y.; Shi, Y. An evaluation of iron ore tailings characteristics and iron ore tailings concrete properties. *Constr. Build. Mater.* **2021**, *286*, 122968. [CrossRef]
6. Zhang, N.; Tang, B.; Liu, X. Cementitious activity of iron ore tailing and its utilization in cementitious materials, bricks and concrete. *Constr. Build. Mater.* **2021**, *288*, 123022. [CrossRef]
7. Duan, P.; Yan, C.; Zhou, W.; Ren, D. Fresh properties, compressive strength and microstructure of fly ash geopolymer paste blended with iron ore tailing under thermal cycle. *Constr. Build. Mater.* **2016**, *118*, 76–88. [CrossRef]
8. Kuranchie, F.A.; Shukla, S.K.; Habibi, D. Utilisation of iron ore mine tailings for the production of geopolymer bricks. *Int. J. Min. Reclam. Environ.* **2016**, *30*, 92–114. [CrossRef]
9. Sant'ana Filho, J.N.; da Silva, S.N.; Silva, G.C.; Mendes, J.C.; Peixoto, R.A.F. Technical and environmental feasibility of interlocking concrete pavers with iron ore tailings from tailings dams. *J. Mater. Civ. Eng.* **2017**, *29*, 04017104. [CrossRef]

10. Tataranni, P. Recycled waste powders for alkali-activated paving blocks for urban pavements: A full laboratory characterization. *Infrastructures* **2019**, *4*, 73. [CrossRef]
11. Hossiney, N.; Sepuri, H.K.; Mohan, M.K.; Chandra, S.K.; Kumar, S.L.; Thejas, H.K. Geopolymer concrete paving blocks made with recycled asphalt pavement aggregates towards sustainable urban mobility development. *Cogent Eng.* **2020**, *7*, 1824572. [CrossRef]
12. *ASTM C936/C936M-26*; Standard Specification for Solid Concrete Interlocking Paving Units. ASTM International: West Conshohocken, PA, USA, 2026.
13. *EN 1338:2003*; Concrete Paving Blocks—Requirements and Test Methods. European Committee for Standardization: Brussels, Belgium, 2003.
14. Duxson, P.; Fernández-Jiménez, A.; Provis, J.L.; Lukey, G.C.; Palomo, A.; van Deventer, J.S.J. Geopolymer technology: The current state of the art. *J. Mater. Sci.* **2007**, *42*, 2917–2933. [CrossRef]
15. Provis, J.L. Geopolymers and other alkali activated materials: Why, how, and what? *Mater. Struct.* **2014**, *47*, 11–25. [CrossRef]
16. Provis, J.L.; Palomo, A.; Shi, C. Advances in understanding alkali-activated materials. *Cem. Concr. Res.* **2015**, *78*, 110–125. [CrossRef]
17. Zhao, S.; Fan, J.; Sun, W. Utilization of iron ore tailings as fine aggregate in ultra-high performance concrete. *Constr. Build. Mater.* **2014**, *50*, 540–548. [CrossRef]
18. Shettima, A.U.; Hussin, M.W.; Ahmad, Y.; Mirza, J. Evaluation of iron ore tailings as replacement for fine aggregate in concrete. *Constr. Build. Mater.* **2016**, *120*, 72–79. [CrossRef]
19. Fontes, W.C.; Mendes, J.C.; da Silva, S.N.; Peixoto, R.A.F. Mortars for laying and coating produced with iron ore tailings from tailing dams. *Constr. Build. Mater.* **2016**, *112*, 988–995. [CrossRef]
20. Tang, C.; Li, K.; Ni, W.; Fan, D. Recovering iron from iron ore tailings and preparing concrete composite admixtures. *Minerals* **2019**, *9*, 232. [CrossRef]
21. Zhang, W.; Gu, X.; Qiu, J.; Liu, J.; Zhao, Y.; Li, X. Effects of iron ore tailings on the compressive strength and permeability of ultra-high performance concrete. *Constr. Build. Mater.* **2020**, *260*, 119917. [CrossRef]
22. Protasio, F.N.M.; de Avillez, R.R.; Letichevsky, S.; Silva, F.A. The use of iron ore tailings obtained from the Germano dam in the production of a sustainable concrete. *J. Clean. Prod.* **2021**, *278*, 123929. [CrossRef]
23. Nematollahi, B.; Sanjayan, J.; Shaikh, F.U.A. Synthesis of heat and ambient cured one-part geopolymer mixes with different grades of sodium silicate. *Ceram. Int.* **2015**, *41*, 5696–5704. [CrossRef]
24. Luukkonen, T.; Abdollahnejad, Z.; Yliniemi, J.; Kinnunen, P.; Illikainen, M. Comparison of alkali and silica sources in one-part alkali-activated blast furnace slag mortar. *J. Clean. Prod.* **2018**, *187*, 171–179. [CrossRef]
25. Adesanya, E.; Ohenoja, K.; Luukkonen, T.; Kinnunen, P.; Illikainen, M. One-part geopolymer cement from slag and pretreated paper sludge. *J. Clean. Prod.* **2018**, *185*, 168–175. [CrossRef]
26. Perumal, P.; Sreenivasan, H.; Luukkonen, T.; Kantola, A.M.; Telkki, V.-V.; Kinnunen, P.; Illikainen, M. High strength one-part alkali-activated slag blends designed by particle packing optimization. *Constr. Build. Mater.* **2021**, *299*, 124004. [CrossRef]
27. Alzaza, A.; Ohenoja, K.; Illikainen, M. One-part alkali-activated blast furnace slag for sustainable construction at subzero temperatures. *Constr. Build. Mater.* **2021**, *276*, 122026. [CrossRef]
28. Mahdi, S.N.; Babu R, D.V.; Hossiney, N.; Abdullah, M.M.A.B. Strength and durability properties of geopolymer paver blocks made with fly ash and brick kiln rice husk ash. *Case Stud. Constr. Mater.* **2022**, *16*, e00800. [CrossRef]
29. Merino-Lechuga, A.M.; Lamaa, G.; Silva, R.V.; de Brito, J.; Jiménez, J.R.; Fernández-Rodríguez, J.M.; González-Caro, Á. Accelerated carbonation of alkali-activated vibro-compacted pervious concrete paving blocks. *Constr. Build. Mater.* **2024**, *449*, 138458. [CrossRef]
30. Merino-Lechuga, A.M.; Lamaa, G.; Silva, R.V.; de Brito, J.; Jiménez, J.R.; Fernández-Rodríguez, J.M.; González-Caro, Á. Technical and environmental assessment of CO_2-cured alkali-activated pervious paving blocks incorporating recycled aggregates. *Constr. Build. Mater.* **2025**, *489*, 142286. [CrossRef]
31. Thejas, H.K.; Hossiney, N. Alkali-activated bricks made with mining waste iron ore tailings. *Case Stud. Constr. Mater.* **2022**, *16*, e00973. [CrossRef]
32. Saldanha, R.B.; Lotero, A.; de Araujo, M.T.; Scheuermann Filho, H.C.; Moncaleano, C.J.; Sousa Silva, J.P.; Consoli, N.C. Potential use of iron ore tailings for binder production: A life cycle assessment. *Constr. Build. Mater.* **2023**, *365*, 130008. [CrossRef]
33. Paniya Parto Kahraba Co. Company and Iron-Concentrate Production Information; Paniya Parto Kahraba Co.: Andimeshk, Iran. Available online: https://paniyasteel.ir/ (accessed on 20 July 2026).
34. *ASTM D2487-17(2025)*; Standard Practice for Classification of Soils for Engineering Purposes (Unified Soil Classification System). ASTM International: West Conshohocken, PA, USA, 2025.
35. Ghasemi, S.; Behnamfard, A.; Arjmand, R. Reprocessing of Sangan iron ore tailings by flotation. *J. Min. Environ.* **2019**, *10*, 729–745. [CrossRef]
36. U.S. Environmental Protection Agency. *SW-846 Method 1311: Toxicity Characteristic Leaching Procedure*; Revision 0; U.S. Environmental Protection Agency: Washington, DC, USA, 1992.

37. Kavussi, A.; Jalili Qazizadeh, M.; Hassani, A. Fatigue behavior analysis of asphalt mixes containing electric arc furnace (EAF) steel slag. *J. Rehabil. Civ. Eng.* **2015**, *3*, 74–86. [CrossRef]
38. FAMCO. *Certificate of Analysis: Solid Sodium Metasilicate Pentahydrate, Supplier Certificate*; FAMCO: Tehran, Iran, 2022.
39. FAMCO. *Certificate of Analysis: Caustic Soda Flakes, Supplier Certificate*; FAMCO: Tehran, Iran, 2022.
40. Nath, P.; Sarker, P.K. Effect of GGBFS on setting, workability and early strength properties of fly ash geopolymer concrete cured in ambient condition. *Constr. Build. Mater.* **2014**, *66*, 163–171. [CrossRef]
41. Ismail, I.; Bernal, S.A.; Provis, J.L.; Nicolas, R.S.; Hamdan, S.; van Deventer, J.S.J. Modification of phase evolution in alkali-activated blast furnace slag by the incorporation of fly ash. *Cem. Concr. Compos.* **2014**, *45*, 125–135. [CrossRef]
42. Ben Haha, M.; Lothenbach, B.; Le Saout, G.; Winnefeld, F. Influence of activator type on hydration kinetics, hydrate assemblage and microstructural development of alkali activated blast-furnace slags. *Cem. Concr. Res.* **2011**, *41*, 301–310. [CrossRef]
43. Walloch, C.; Lang, N.; Smith, D.R. *Compressive Strength Testing of Concrete Paving Units: Research on Configuration of Tested Specimens and Effects of Variables in Specimen Capping*; ASTM International: West Conshohocken, PA, USA, 2014; pp. 1–30. [CrossRef]
44. *ASTM C140/C140M-26a*; Standard Test Methods for Sampling and Testing Concrete Masonry Units and Related Units. ASTM International: West Conshohocken, PA, USA, 2026.
45. *ASTM C78/C78M-22*; Standard Test Method for Flexural Strength of Concrete (Using Simple Beam with Third-Point Loading). ASTM International: West Conshohocken, PA, USA, 2022.
46. *ISO 14040:2006*; Environmental Management—Life Cycle Assessment—Principles and Framework. International Organization for Standardization: Geneva, Switzerland, 2006.
47. *ISO 14044:2006*; Environmental Management—Life Cycle Assessment—Requirements and Guidelines. International Organization for Standardization: Geneva, Switzerland, 2006.
48. *ASTM C136/C136M-25*; Standard Test Method for Sieve Analysis of Fine and Coarse Aggregates. ASTM International: West Conshohocken, PA, USA, 2025.
49. Myers, R.H.; Montgomery, D.C.; Anderson-Cook, C.M. *Response Surface Methodology: Process and Product Optimization Using Designed Experiments*, 4th ed.; Wiley: Hoboken, NJ, USA, 2016.
50. *ACI CODE-318-25*; Building Code Requirements for Structural Concrete and Commentary. American Concrete Institute: Farmington Hills, MI, USA, 2025.
51. Derringer, G.; Suich, R. Simultaneous optimization of several response variables. *J. Qual. Technol.* **1980**, *12*, 214–219. [CrossRef]
52. Bernal, S.A.; Provis, J.L.; Walkley, B.; San Nicolas, R.; Gehman, J.D.; Brice, D.G.; Kilcullen, A.R.; Duxson, P.; van Deventer, J.S.J. Gel nanostructure in alkali-activated binders based on slag and fly ash, and effects of accelerated carbonation. *Cem. Concr. Res.* **2013**, *53*, 127–144. [CrossRef]
53. *ASTM C642-21*; Standard Test Method for Density, Absorption, and Voids in Hardened Concrete. ASTM International: West Conshohocken, PA, USA, 2021.
54. *ASTM C1645-22ae1*; Standard Test Method for Freeze-Thaw and De-Icing Salt Durability of Solid Concrete Interlocking Paving Units. ASTM International: West Conshohocken, PA, USA, 2022.

Disclaimer/Publisher's Note: The statements, opinions and data contained in all publications are solely those of the individual author(s) and contributor(s) and not of MDPI and/or the editor(s). MDPI and/or the editor(s) disclaim responsibility for any injury to people or property resulting from any ideas, methods, instructions or products referred to in the content.